Philosophical Magazine

ISSN: 1478-6435 (Print) 1478-6443 (Online) Journal homepage: http://www.tandfonline.com/loi/tphm20

Revealing the electronic structure and optical properties of $K_6[Mo_4O_8F_{10}]$ novel molybdenum oxyfluoride materials

Ali H. Reshak

To cite this article: Ali H. Reshak (2016): Revealing the electronic structure and optical properties of $K_6[Mo_4O_8F_{10}]$ novel molybdenum oxyfluoride materials, Philosophical Magazine, DOI: 10.1080/14786435.2016.1227879

To link to this article: http://dx.doi.org/10.1080/14786435.2016.1227879

Published online: 31 Aug 2016.

PHILOSOPHICAL MAGAZINE, 2016
http://dx.doi.org/10.1080/14786435.2016.1227879

Taylor & Francis
Taylor & Francis Group

Revealing the electronic structure and optical properties of $K_6[Mo_4O_8F_{10}]$ novel molybdenum oxyfluoride materials

Ali H. Reshak[a,b]

[a]New Technologies – Research Centre, University of West Bohemia, Pilsen, Czech Republic; [b]School of Material Engineering, University Malaysia Perlis, Kangar, Malaysia

ABSTRACT

The electronic structure and optical properties of the molybdenum oxyfluoride $K_6[Mo_4O_8F_{10}]$ single crystal were investigated. Based on X-ray diffraction data, the crystal structure was optimised so as to minimise the forces acting on each atom. The calculation reveal that $K_6[Mo_4O_8F_{10}]$ is an indirect band gap semiconductor of about 1.51 eV, using the local density approximation, 1.72 eV, using gradient approximation (PBE-GGA), 1.81 eV using Engel–Vosko generalized gradient approximation and 2.01 eV, from the recently modified Becke–Johnson potential (TB-GGA-mBJ). Partial density of states reveals the orbitals' contribution and the degree of the hybridisations between the orbitals. The contours of the valence electronic charge density of each atom in $K_6[Mo_4O_8F_{10}]$ reveal that there are some electrons from Mo, K, F and O orbitals that are transferred to the valence bands and participate in the interactions between the Mo, K, F and O atoms to form covalent bonding. The strength of the covalent bond depends on the degree of the hybridisation and the electro-negativity differences between Mo, K, F and O atoms. The calculated bond lengths exhibit good agreement with the experimental data. The optical properties help to get deep insight into the electronic structure and reveal the types of the orbitals that participate in the optical transitions. It has been found that the investigated crystal possesses negative uniaxial anisotropy ($\delta\varepsilon = -0.102$) and positive birefringence ($\Delta n(0) = 0.2765$).

ARTICLE HISTORY
Received 9 May 2016
Accepted 18 August 2016

KEYWORDS
Electronic materials; fullerenes; ab initio; optical properties

1. Introduction

Several synthetic methods have been most frequently used since 1985 in different fields of the broad area of preparative inorganic fluorine chemistry, emphasising those routes which have had and still may have an impact on future progress. Attention is focused on developments that have led to actual or potential routes to new fluoride materials [1]. The high electro-negativity and the small-size of F-ligand, combined with the low bond energy in F_2 and the strong bonds that F-ligand makes with most other atoms, are the fundamental characteristics that lie at the basis of the ready combustion of most of the elements in fluorine, often resulting in their oxidation to the highest known state of oxidation. Fluoride

CONTACT Ali H. Reshak maalidph@yahoo.co.uk

synthesis in the past, at least in its inorganic aspects, was often simply a matter of heating materials in F_2 (sometimes under pressure). Today's picture is dramatically different [2]. Maggard et al. [3] have synthesised $(Ag_3MoO_3F_3)(Ag_3MoO_4)Cl$ single crystals by hydro-solvatothermal methods and characterised them by X-ray diffraction (XRD). They obtain transparent colourless crystals. Lin et al. [4] have synthesised new pyrazine-pillared solids, $AgReO_4(C_4H_4N_2)$ (I) and $Ag_3Mo_2O_4F_7(C_4H_4N_2)_3$ ($C_4H_4N_2$ = pyrazine, pyz) (II), by hydro-thermal methods at 150 °C and also characterised them using single-crystal XRD. They analysed the structural properties of the investigated materials and calculated the electronic band structure based on density functional theory (DFT). In recent years, new structural units in molybdenum oxyfluoride chemistry have been reported [2,5–10]. Recently Aldous and Lightfoot [2] have presented the solvothermal syntheses and crystal structures of five new molybdenum oxyfluorides; they reported that the new molybdenum oxyfluorides show three novel structural units which contain Mo in a reduced oxidation state. Moreover, they observed the Mo-Mo bonds in each unit [2,5–10].

Due to the novelty and the lack of information concerning the electronic structural information on $K_6[Mo_4O_8F_{10}]$ molybdenum oxyfluoride single crystals, further insight into the electronic structure can be obtained from the electronic band structure, the density of states, the electronic charge density distribution and the optical properties. Therefore, this study is aimed at performing comprehensive full potential calculations based on the DFT within several possibilities of exchange-correlation (XC) potentials to ascertain the effect of exchange correlation on the ground state properties of the $K_6[Mo_4O_8F_{10}]$ molybdenum oxyfluoride single crystal. Since there is no information concerning the experimental band gap, based on our experiences with the recently modified Becke–Johnson potential (mBJ), we believe that the calculated band gap using mBJ would be close to the expected experimental energy gap. Recently it has been found that the first-principles calculation is one powerful and useful tool to predict the crystal structure and its properties related to the electron configuration of a material before its synthesis [11–14].

2. Details of calculations

Molybdenum oxyfluoride $K_6[Mo_4O_8F_{10}]$ single crystals were recently synthesised by Aldous and Lightfoot [2]. It has been reported that $K_6[Mo_4O_8F_{10}]$ crystallises in an orthorhombic structure, space group, *Pnnm* (No. 58) with two formulae per unit cell. The unit cell parameters are $a = 6.0483(7)$ Å, $b = 9.351(1)$ Å, $c = 14.487(2)$ Å, $\alpha = \beta = \gamma = 90^{\circ}$ and $V = 819.4(2)$ Å^3 [2]. The molybdenum oxyfluoride $K_6[Mo_4O_8F_{10}]$ single crystal is a highly fluorinated tetrameric unit in MoOF [2]. Figure 1 illustrates the crystal structure of a molybdenum oxyfluoride $K_6[Mo_4O_8F_{10}]$ single crystal. The atomic positions have been optimised by minimising the forces (1*mRy*/*a.u.*) acting on the atoms. The generalised gradient approximation (PBE-GGA) was used to achieve the optimisation. The optimised atomic positions agree well with the experimental ones [2]; these are listed in Table 1. The DFT within the full-potential linear augmented-plane-wave (FPLAPW+lo) method in a scalar relativistic version as embodied in the WIEN2k code [15] was used to perform comprehensive calculations for the electronic band structure, the density of states, the space electronic charge density and the optical properties of a $K_6[Mo_4O_8F_{10}]$ molybdenum oxyfluoride single crystal. It is well known that in the DFT calculation the exact form of the XC functional is unknown. Therefore, the accuracy of the results will be sensitive to selection of the XC functional and it

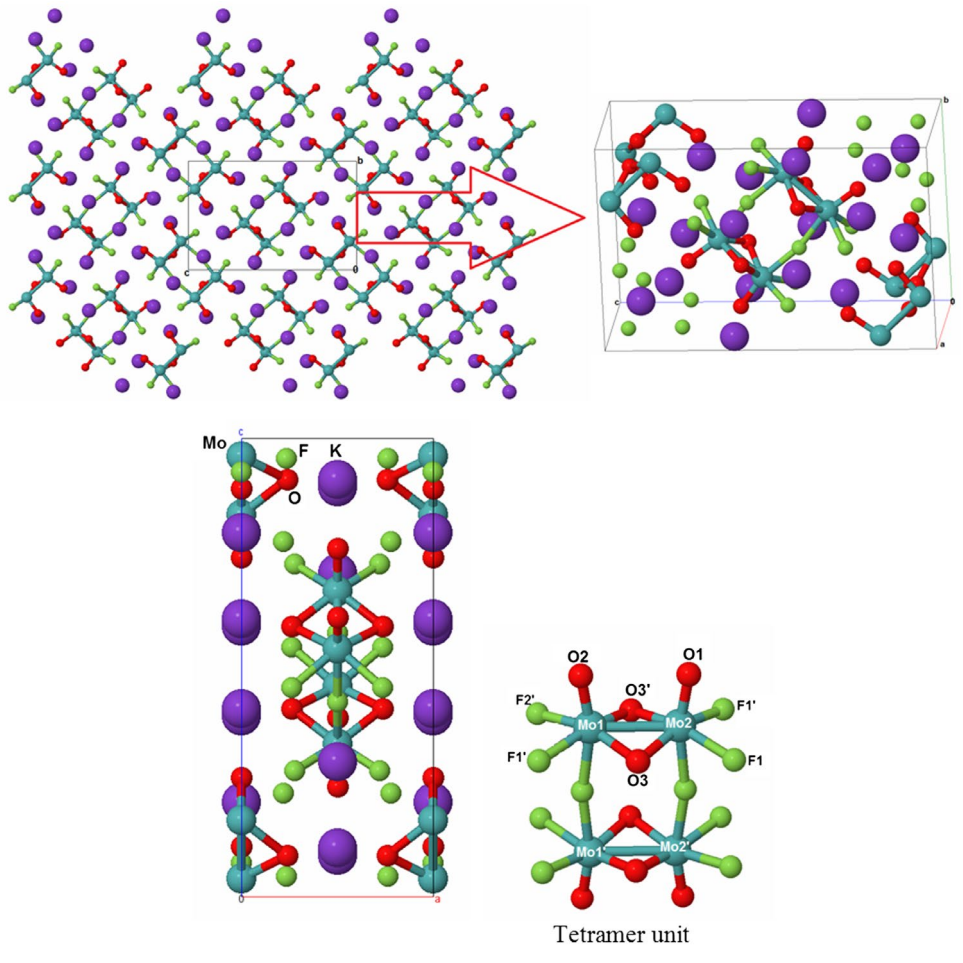

Figure 1. (colour online) The crystal structure of $K_6[Mo_4O_8F_{10}]$ single crystal.

Table 1. Calculated atomic positions in comparsion with the experimental data [2].

Atom	*x*-exp.	*x*-opt.	*y*-exp.	*y*-opt.	*z*-exp.	*z*-opt.
Mo1	0.0000	0.0000	0.06939(7)	0.07234	0.16627(5)	0.16645
Mo2	0.0000	0.0000	0.25852(7)	0.26012	0.04026(4)	0.04232
K3	0.0000	0.0000	−0.0670(2)	0.93311	0.39399(13)	0.39125
K1	0.0000	0.0000	−0.34067(19)	0.65933	0.20564(13)	0.21000
K2	−0.5000	0.5000	−0.12457(19)	0.87543	0.09012(12)	0.09122
F1	0.2366(6)	0.2411	0.3414(3)	0.34998	0.3414(3)	0.34162
F2	0.2208(6)	0.2232	−0.0632(3)	0.93681	0.2258(2)	0.22611
F3	0.0000	0.0000	−0.1117(5)	0.88831	0.0744(3)	0.07551
O1	0.0000	0.0000	0.4024(6)	0.41354	0.1096(4)	0.10987
O2	0.0000	0.0000	0.1761(6)	0.1758	0.2603(4)	0.26111
O3	0.2381(7)	0.2411	0.1410(4)	0.1411	0.0897(3)	0.08956

can play a major role in the accuracy of the results; this is one of the main drawbacks in DFT. Thus, in the current calculations the XC potential problem was solved using four different possible approximations. The XC potentials used here are; the local density approximation (LDA) [16] and the PBE-GGA [17], which are based on XC energy optimisation to calculate

the total energy. It is well known that in calculating the self-consistent band structure within DFT, the LDA and GGA underestimate the energy band gap by around 10–30% [18–20]. This is mainly due to the fact that LDA and GGA have simple forms that are not sufficiently flexible to accurately reproduce both the XC energy and its charge derivative. Engel and Vosko [21] considered this shortcoming and constructed a new functional form, GGA, that is able to better reproduce the exchange potential at the expense of less agreement in the exchange energy. This approach, called Engel–Vosko generalised gradient approximation (EV-GGA), yields better band splitting and some other properties that mainly depend on the accuracy of the XC potential. In addition, the recently modified Becke–Johnson potential (mBJ) [22] have been used, which optimises the corresponding potential for electronic band structure calculations and hence the energy band gap.

The Kohn–Sham equations are solved using a basis of linear APW's. The potential and charge density in the muffin-tin (MT) spheres are expanded in spherical harmonics with $l_{max} = 8$ and nonspherical components up to $l_{max} = 6$. In the interstitial region, the potential and the charge density are represented by Fourier series. Self-consistency is obtained using 300 $\vec{k}$ points in the irreducible Brillouin zone (IBZ). The electronic band structure, density of states, electronic charge density distribution and linear optical properties have been calculated, using 800 $\vec{k}$ points in the IBZ. The self-consistent calculations are converged, since the total energy of the system is stable within 0.01 mRy.

3. Results and discussion

3.1. Electronic band structure and density of states

To ascertain the effect of XC on the band splitting and hence on the value of the energy band gap, four different types of XC potentials were employed to calculate the electronic band structure of the $K_6[Mo_4O_8F_{10}]$ molybdenum oxyfluoride single crystal. These are LDA, PBE-GGA, EV-GGA and TB-GGA-mBJ. For all cases, the zero-point of energy was set at the valence band maximum (VBM). The conduction band minimum (CBM) is located at the centre (Γ) of BZ, while the VBM is situated at the U point of BZ, resulting in an indirect band gap of about 1.51 eV (LDA), 1.72 eV (PBE-GGA), 1.81 eV(EV-GGA) and 2.01 eV (TB-GGA-mBJ). To the best of our knowledge, there are no previous experimental or theoretical data for the energy band gap available in literature to make a meaningful comparison. Therefore, based on our experiences in using different XC functional (LDA, PBE-GGA, EV-GGA and mBJ) on several compounds whose energy band gaps are known experimentally [23], in those previous calculations we found that the mBJ gives very good agreement with experimental data [23]. This motivated us to use mBJ to calculate the band structure and hence the optical properties of $K_6[Mo_4O_8F_{10}]$. The mBJ is a modified Becke–Johnson potential which allows the calculation of the energy band gap with accuracy similar to the very expensive GW calculations [22]. It is a local approximation to an atomic 'exact-exchange' potential and a screening term. Thus, we believe that the calculated energy band gap reported in this paper would be close to the expected experimental energy band gap. Future experimental work will confirm the calculated results. Therefore, we will present only the results obtained by mBJ. Figure 2 illustrates the calculated electronic band structure and the total density of states of the molybdenum oxyfluoride $K_6[Mo_4O_8F_{10}]$ single crystal.

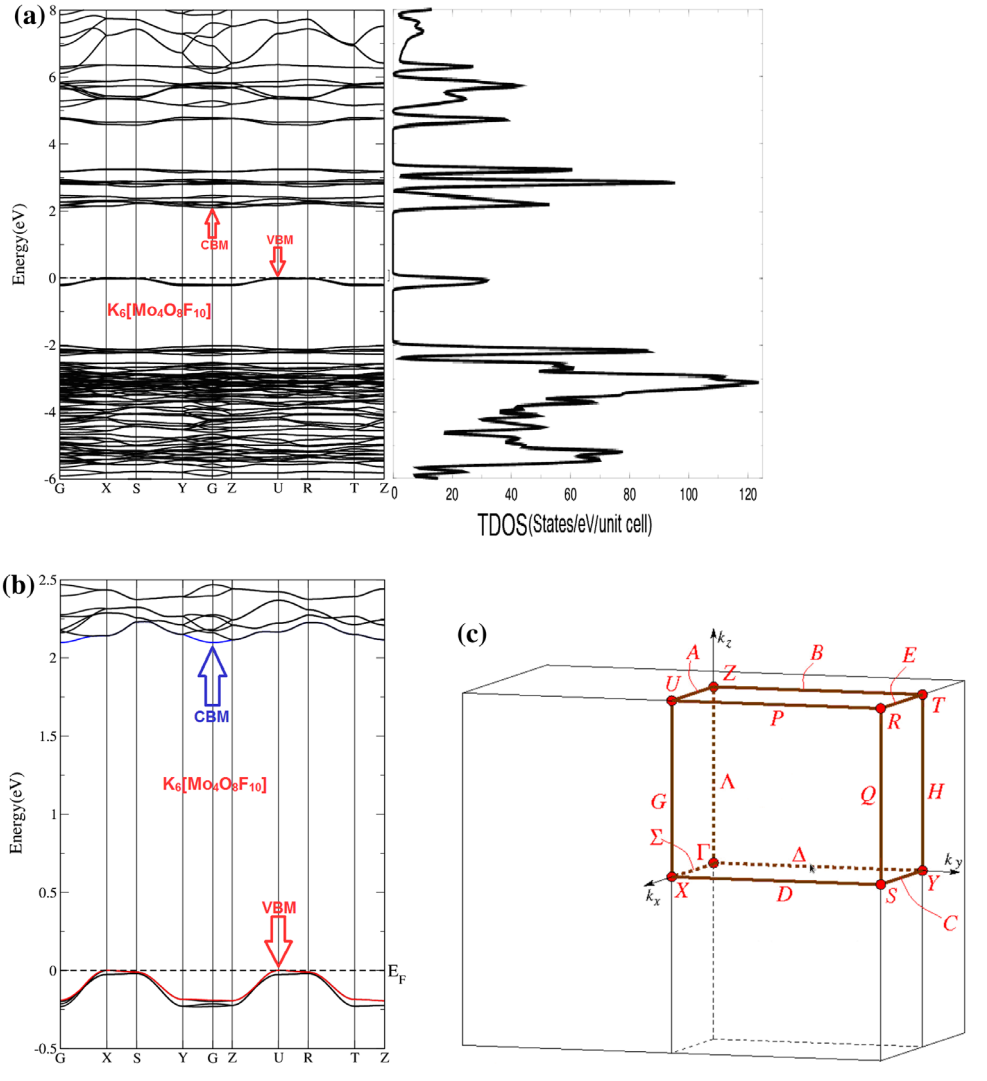

Figure 2. (colour online) (a) The calculated electronic band structure of $K_6[Mo_4O_8F_{10}]$ single crystal along with total density of states using mBJ; (b) Enlarged electronic band structure of $K_6[Mo_4O_8F_{10}]$ in the energy range between 2.5 and −0.5 eV to clearly show the VBM and the CBM, therefore we coloured the VBM by red and the CMB by blue. The colours of the VBM and the CBM means nothing just to indicate them from the others; (c) the BZ of $K_6[Mo_4O_8F_{10}]$.

The Mo-5s/4p/4d, K-4s/3p, F-2s/2p and O-2s/2p partial density of states (PDOS) are illustrated in Figure 3(a)–(d). It is evident that the VBM mainly originates from the Mo1-d, Mo2-d and O3-p states with a small contribution from O2-p, F2-p and O3-s states, whereas the CBM originates from Mo1-d, Mo2-d, O2-p and O3-p states with a small contribution from F2-p, F3-s and O3-s states. It is interesting to mention that the O-2s orbitals extended along the whole energy range along with F-2s, Mo-5s/4p and K-4s orbitals to form a strong/weak hybridisation. While O-2p orbitals confined between −7.0 eV and +7.0 eV share the same area with Mo-4d and F-2p orbitals and form strong/weak hybridisations. The K-3p orbital is situated around −13.0 eV and exhibits a very sharp structure.

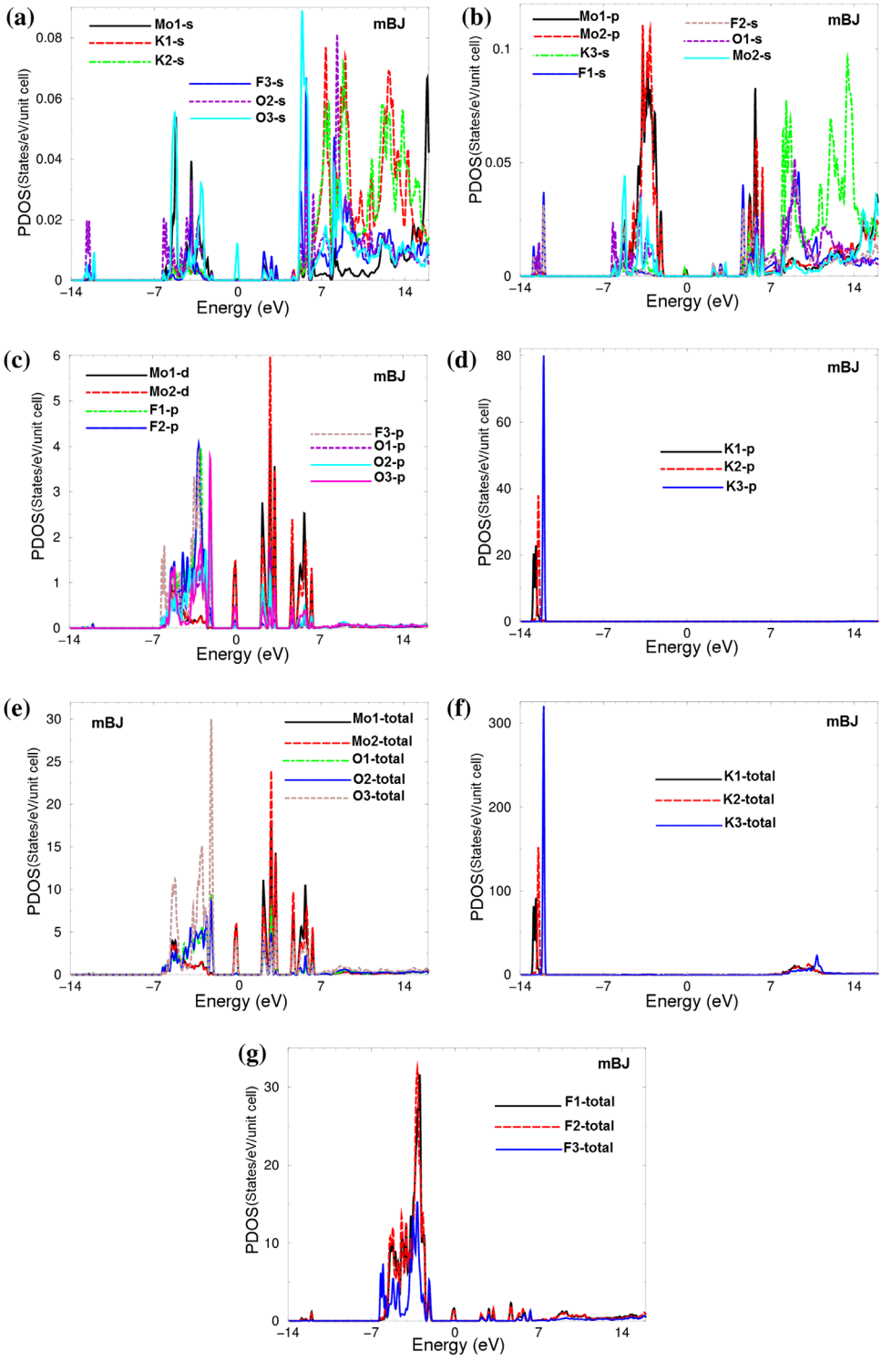

Figure 3. (colour online) (a–g) Calculated PDOS (states/eV/ unit cell) using mBJ.

Table 2. Calculated bond lengths in comparsion with the experimental data [2].

Bonds	Exp. bond lengths (Å)	Calc. bond lengths (Å)
Mo1–O1	1.689 (6)	1.690
Mo1–O3	1.938 (4)	1.940
Mo1–O3′	1.938 (4)	1.940
Mo1–F1	2.016 (3)	2.015
Mo1–F1′	2.016 (3)	2.015
Mo1–F3	2.153 (5)	2.155
Mo2–O2	1.679 (6)	1.680
Mo2–O3	1.948 (4)	1.946
Mo2–O3′	1.948 (4)	1.946
Mo2–F2	2.041 (3)	2.040
Mo2–F2′	2.041 (3)	2.040
Mo2–F3	2.156 (4)	2.157
Mo1–Mo2	2.542 (1)	2.543

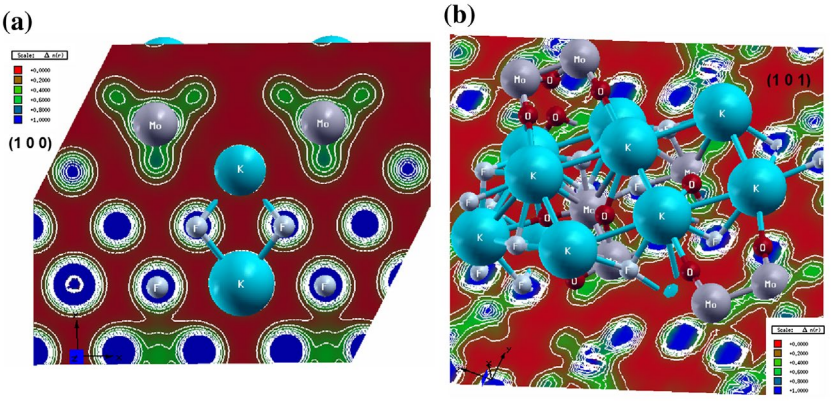

Figure 4. (colour online) The electron charge density distribution of $K_6[Mo_4O_8F_{10}]$ single crystal were calculated for; (a) (1 0 0) crystallographic plane and (b) (1 0 1) crystallographic plane.

In order to elucidate the characteristics of chemical bonding of $K_6[Mo_4O_8F_{10}]$, the calculated PDOS was used. The PDOS spectral structure that extended from −6.0 eV up to E_F is formed by Mo1, 2-5s/4p/4d, O1, 2, 3-2s/2p, F1, 2, 3-2s/2p and K1, 2-4s states. In this energy region, a total number of electrons/electron Volts (e/eV) for each orbital of $K_6[Mo_4O_8F_{10}]$ atoms have been obtained. The F1-2p state 4.1 e/eV, F2-2p state 4.2 e/eV, F3-2p state 4.1 e/eV, F1-2s state 0.02 e/eV, F2-2s state 0.024 e/eV, F3-2s state 0.058 e/eV, Mo1-4d and Mo2-4d states 1.5 e/eV, Mo1-5s state 0.07 e/eV, Mo2-5s state 0.04 e/eV, Mo1-4p state 0.11 e/eV, Mo2-4p state 0.12 e/eV, O1-2p state 1.7 e/eV, O2-2p state 1.8 e/eV, O3-2p state 4.0 e/eV, O1-2s state 0.025 e/eV, O2-2s state 0.037 e/eV, O3-2s state 0.058 e/eV, K1-4s state 0.013 e/eV, K2-4s state 0.012 e/eVand K3-4s state 0.01 e/eV. Therefore, it is clear that some electrons from these orbitals are transferred to the VBs and participate in the interactions between the Mo, K, F and O atoms to form covalent bonding. The strength of the covalent bond depends on the degree of the hybridisation and the electro-negativity differences between Mo, K, F and O atoms. This can be seen directly from the contours of the valence electronic charge density of each atom in $K_6[Mo_4O_8F_{10}]$. We have obtained these contours in two planes along (1 0 0) and (1 0 1) directions, as shown in Figure 4(a) and (b). From the (1 0 0) crystallographic plane, it can be seen that the Mo atom forms strong covalent bonds with the nearest three O atoms, while F and K atoms form pure ionic bonds, as

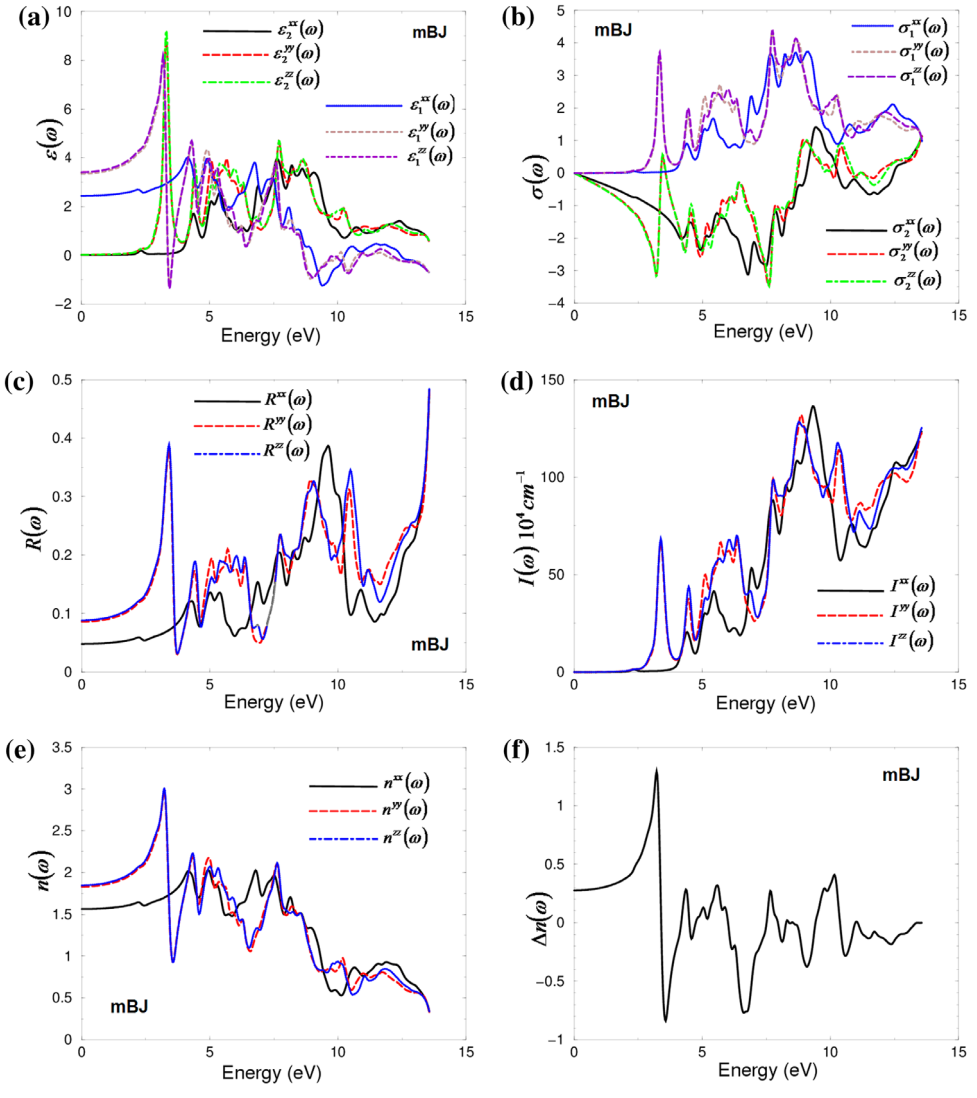

Figure 5. (colour online) (a) Calculated $\varepsilon_2^{xx}(\omega)$ (dark solid curve-black colour online), $\varepsilon_2^{yy}(\omega)$ (light long dashed curve-red colour online) and $\varepsilon_2^{zz}(\omega)$ (light dotted dashed curve-green colour online) along with calculated $\varepsilon_1^{xx}(\omega)$ (dark solid curve-blue colour online), $\varepsilon_1^{yy}(\omega)$ (light dashed curve-brown colour online) and $\varepsilon_1^{zz}(\omega)$ (light sold curve -violet colour online) of $K_6[Mo_4O_8F_{10}]$ single crystal; (b) Calculated $\sigma_2^{xx}(\omega)$ (dark solid curve-black colour online), $\sigma_2^{yy}(\omega)$ (light long dashed curve-red colour online) and $\sigma_2^{zz}(\omega)$ (light dotted dashed curve-green colour online) along with calculated $\sigma_1^{xx}(\omega)$ (dark solid curve-blue colour online), $\sigma_1^{yy}(\omega)$ (light dashed curve-brown colour online) and $\sigma_1^{zz}(\omega)$ (light sold curve -violet colour online) of $K_6[Mo_4O_8F_{10}]$ single crystal; (c) Calculated refractive indices $R^{xx}(\omega)$ (dark solid curve-black colour online), $R^{yy}(\omega)$ (light dashed curve-red colour online) and $R^{zz}(\omega)$ (light dotted dashed curve -blue colour online) spectrum of $K_6[Mo_4O_8F_{10}]$ single crystal; (d) Calculated refractive indices $I^{xx}(\omega)$ (dark solid curve-black colour online), $I^{yy}(\omega)$ (light dashed curve-red colour online) and $I^{zz}(\omega)$ (light dotted dashed curve-blue colour online) spectrum of $K_6[Mo_4O_8F_{10}]$ single crystal; (e) Calculated refractive indices $n^{xx}(\omega)$ (dark solid curve-black colour online), $n^{yy}(\omega)$ (light dashed curve-red colour online) and $n^{zz}(\omega)$ (light dotted dashed curve -blue colour online) spectrum of $K_6[Mo_4O_8F_{10}]$ single crystal; (f) Calculated birefringence $\Delta n(\omega)$ of $K_6[Mo_4O_8F_{10}]$ single crystal.

Table 3. Calculated $\varepsilon_1^{xx}(0)$, $\varepsilon_1^{yy}(0)$, $\varepsilon_1^{zz}(0)$, $\delta\varepsilon$, ω_p^{xx}, ω_p^{yy}, ω_p^{zz}, $n^{xx}(\omega)$, $n^{yy}(\omega)$, $n^{zz}(\omega)$ and $\Delta n(\omega)$.

	LDA	GGA	EVGGA	mBJ
$\varepsilon_1^{xx}(0)$	2.647	2.570	2.500	2.441
$\varepsilon_1^{yy}(0)$	3.524	3.538	3.510	3.351
$\varepsilon_1^{zz}(0)$	3.612	3.624	3.595	3.413
$\delta\varepsilon$	−0.094	−0.103	−0.109	−0.102
ω_p^{xx}	9.020	9.075	9.075	9.075
ω_p^{yy}	8.476	8.557	8.623	8.721
ω_p^{zz}	8.476	8.530	8.567	8.694
$n^{xx}(0)$	1.627	1.603	1.542	1.562
$n^{yy}(0)$	1.877	1.881	1.811	1.830
$n^{zz}(0)$	1.900	1.903	1.856	1.847
$\Delta n(0)$	0.261	0.289	0.291	0.2765

they are surrounded by uniform spheres. Charge transfer occurs toward F atoms, which is attributed to the fact that F atoms possess the highest electro-negatively among the others. More details can be seen from the (1 0 1) crystallographic plane, which reveals the strong covalent bonds between Mo and F atoms. This supports the finding from the PDOS, which states that there exists a strong hybridisation between Mo, O and F atoms. The strong/weak hybridisation may lead to the formation of strong/weak covalent bonding. It is interesting to compare our calculated bond lengths with the measured ones [2], as shown in Table 2, which reveals that there is a good agreement between the theory and experiment.

3.2. Linear optical properties

Since the optical dielectric functions involve the energy eigenvalues and electron wave functions, they are natural outputs of the electronic band structure. Therefore, we utilised the calculated optical dielectric functions to further reveal the origin of the electronic band structure of a $K_6[Mo_4O_8F_{10}]$ single crystal. Figure 5(a) illustrates the calculated imaginary and real parts of the optical dielectric functions, which show that the absorption edge occurs at 2.098 eV. The two optical components along the polarisation directions [0 1 0] and [0 0 1] exhibit a sharp peak around 3.0 eV; the strength of this peak can be explained due to the fact that $\varepsilon_2(\omega)$ scales as $1/\omega^2$. While the optical components along the [1 0 0] polarisation direction show no contribution to the optical spectra up to 4.0 eV. The two optical components $\varepsilon_2^{yy}(\omega)$ and $\varepsilon_2^{zz}(\omega)$ exhibit a considerable anisotropy with $\varepsilon_2^{xx}(\omega)$. To analyse the origin of the optical spectral structure, we have used our calculated angular momentum resolved projected density of states which enables us to identify the angular momentum characteristics of the various structures that are responsible for the optical structure. The absorption edges belong to the optical transitions between Mo-5s/4d, O-2s/2p states (VBs) and Mo-5s/4p, O-2s/2p, F-2s states (CBs). The optical spectra above the absorption edges originate from transitions between Mo-5s/4p/4d, O-2s/2p, K-4s, F-2p states (VBs) and Mo-5s/4p/4d, O-2p, F-2s/2p states (CBs).

From the imaginary part, the real part is obtained by means of the Kramers–Kronig transformation [24]. It is clear that $\varepsilon_1^{yy}(\omega) = \varepsilon_1^{zz}(\omega)$ and shows considerable anisotropy with $\varepsilon_1^{xx}(\omega)$, which shows that $K_6[Mo_4O_8F_{10}]$ is a uniaxial crystal. The vanishing frequency value of the dielectric function which defines the static electronic dielectric constant $\varepsilon_\infty = \varepsilon_1(\omega = 0)$can be obtained from $\varepsilon_1^{xx}(0)$, $\varepsilon_1^{yy}(0)$ and $\varepsilon_1^{zz}(0)$, as shown in Table 3. With the aid of these values,

we can estimate the value of the energy gap following the Penn model [25] and the uniaxial anisotropy ($\delta\varepsilon = \left[(\varepsilon_0^{\mathrm{II}} - \varepsilon_0^{\perp})/\varepsilon_0^{\mathrm{tot}}\right]$). The obtained $\delta\varepsilon$ value shows that this crystal possesses negative uniaxial anisotropy. Furthermore, the plasmon oscillations ω_p^{xx}, ω_p^{yy} and ω_p^{zz}, which are associated with the existence of plasma oscillations (plasmons), can be obtained at the energies where $\varepsilon_1^{xx}(\omega)$, $\varepsilon_1^{yy}(\omega)$ and $\varepsilon_1^{zz}(\omega)$ cross zero. These values are given in Table 3.

The optical conductivity, as illustrated in Figure 5(b), is obtained from the imaginary and real parts of the optical dielectric functions $\varepsilon(\omega) = \varepsilon_1(\omega) + i\varepsilon_2(\omega) = 1 + 4\pi i\sigma(\omega)/\omega$. It can be seen that $\sigma^{yy}(\omega) = \sigma^{zz}(\omega)$ shows considerable anisotropy with $\sigma^{xx}(\omega)$, which confirms the previous observation from Figure 5(a). The optical conductivity spectral structure (Figure 5(c)) is determined by the electric-dipole transitions between the occupied valence bands and the unoccupied conduction bands. The calculated optical reflectivity of the $K_6[Mo_4O_8F_{10}]$ single crystal shows low reflectivity in the low-energy region ($R^{xx}(\omega) = 5.0\%$, $R^{yy}(\omega) = R^{zz}(\omega) = 9.0\%$). Increasing the photon energy leads to an increase in the reflectivity of $R^{yy}(\omega) = R^{zz}(\omega)$ to reach 40.0% at about 3.0 eV, forming the first reflectivity maxima. It has been found that there is an abrupt reduction in the reflectivity spectrum at 11.5 eV for the three components $R^{xx}(\omega)$, $R^{yy}(\omega)$ and $R^{zz}(\omega)$, confirming the occurrence of a collective plasmon resonance. The depth of the plasmon minimum is determined by $\varepsilon_2(\omega)$ at the plasma resonance, which represents the degree of the overlap between the inter-band absorption regions.

The absorption coefficient of the $K_6[Mo_4O_8F_{10}]$ single crystal as a function of photon energy is shown in Figure 5(d). The spectra demonstrate the location of the absorption edges which occur between the top of the VB and the bottom of the CB. After the absorption edges, the component $I^{yy}(\omega) = I^{zz}(\omega)$ exhibits a rapid and sharp absorption, while the $I^{xx}(\omega)$ component rises at around 4.0 eV. The maximum absorption occurs at around 9.0 eV. The calculated refractive indices, as shown in Figure 5(e), confirm the existence of the considerable anisotropy, and from $n(0)$, the value of the energy band gap ($n = \sqrt{\varepsilon}$) can be estimated. Furthermore, the values of the birefringence $\Delta n(\omega) = n_e(\omega) - n_o(\omega)$, can be obtained from $n^{xx}(\omega)$, $n^{yy}(\omega)$ and $n^{zz}(\omega)$, as shown in Figure 5(f) and Table 3.

4. Conclusions

The calculated electronic band structure of the molybdenum oxyfluoride $K_6[Mo_4O_8F_{10}]$ single crystal shows that the CBM is located at the centre of the BZ, while the VBM at U point of BZ resulting in an indirect band gap. It is evident that the VBM mainly originates from Mo1-d, Mo2-d and O3-p states with small contribution from O2-p, F2-p and O3-s states, whereas the CBM is originated from Mo1-d, Mo2-d, O2-p and O3-p states with a small contribution from F2-p, F3-s and O3-s states. The calculated electronic charge density distribution reveals that a charge transfer occurs toward F atoms, which is attributed to the fact that F atoms possess the highest electro-negativety among the others. Also, it explores the strong covalent bonds between Mo and F atoms. The optical properties reveal that this crystal possesses a negative uniaxial anisotropy ($\delta\varepsilon = -0.102$) and positive birefringence ($\Delta n(0) = 0.2765$). The calculated optical properties reveal the electronic band structure of the molybdenum oxyfluoride $K_6[Mo_4O_8F_{10}]$ single crystal.

Acknowledgements

The result was developed within the CENTEM project, reg. no. CZ.1.05/2.1.00/03.0088, co-funded by the ERDF as part of the Ministry of Education, Youth and Sports OP RDI programme and, in the follow-up sustainability stage, supported through CENTEM PLUS (LO1402) by financial means from the Ministry of Education, Youth and Sports under the 'National Sustainability Program I'. Computational resources were provided by MetaCentrum (LM2010005) and CERIT-SC (CZ.1.05/3.2.00/08.0144) infrastructures.

Disclosure statement

No potential conflict of interest was reported by the author.

Funding

This work was supported by CENTEM [CZ.1.05/2.1.00/03.0088].

References

[1] T. Nakajima, B. Zemva, and A. Tressaud (eds.), *Advanced Inorganic Fluorides*, Elsevier, Lausanne, 2000.
[2] D.W. Aldous and P. Lightfoot, *New structural units in molybdenum oxyfluoride chemistry*, J. Fluorine Chem. 144 (2012), pp. 108–113.
[3] P.A. Maggard, T.S. Nault, C.L. Stern, and K.R. Poeppelmeier, *Alignment of acentric $MoO_3F_3^{3-}$ anions in a polar material: $(Ag_3MoO_3F_3)(Ag_3MoO_4)Cl$*, J. Solid State Chem. 175 (2003), pp. 27–33.
[4] H. Lin, B. Yan, P.D. Boyle, and P.A. Maggard, *Synthesis and properties of pyrazine-pillared $Ag_3Mo_2O_4F_7$ and $AgReO_4$ layered phases*, J. Solid State Chem. 179 (2006), pp. 217–225.
[5] D.W. Aldous, N.F. Stephens, and P. Lightfoot, *Hydrothermal chemistry of oligomeric vanadium oxyfluorides*, Dalton Trans. 22 (2007), pp. 2271–2282.
[6] D.W. Aldous, R.J. Goff, J.P. Attfield, and P. Lightfoot, *Novel vanadium (IV) oxyfluorides with 'spin-ladder'-like structures, and their relationship to (VO)2P2O7*, Inorg. Chem. 46 (2007), pp. 1277–1282.
[7] D.W. Aldous, N.F. Stephens, and P. Lightfoot, *The role of temperature in the solvothermal synthesis of hybrid vanadium oxyfluorides*, Dalton Trans. 37 (2007), pp. 4207–4213.
[8] K. Adil, M. Leblanc, V. Maisonneuve, and P. Lightfoot, *Structural chemistry of organically-templated metal fluorides*, Dalton Trans. 39 (2010), pp. 5983–5993.
[9] F. Himeur, P.K. Allan, S.J. Teat, R.J. Goff, R.E. Morris, and P. Lightfoot, *Increasing the dimensionality of hybrid vanadium oxyfluorides using ionothermal synthesis*, Dalton Trans. 39 (2010), pp. 6018–6020.
[10] F.H. Aidoudi, D.W. Aldous, R.J. Goff, A.M.Z. Slawin, J.P. Attfield, R.E. Morris, and P. Lightfoot, *An ionothermally prepared S = 1/2 vanadium oxyfluoride kagome lattice*, Nat. Chem. 3 (2011), pp. 801–806.
[11] M. Malachowski, I.R. Kityk, and B. Sahraoui, *Electronic structure and optical response in $Ga_xAl_{1-x}N$ solid alloys*, Phys. Lett. A 242 (1998), pp. 337–342.
[12] I. Fuks-Janczarek, R. Miedzinski, M.G. Brik, A. Majchrowski, L.R. Jaroszewicz, and I.V. Kityk, *First-principles calculations of the structural, electronic, optical and elastic properties of the new phosphors, Na_2ZrF_6 and K_2ZrF_6*, Solid State Sci. 27 (2014), pp. 30–35.
[13] M. Abudoureheman, L. Wang, X. Zhang, H. Yu, Z. Yang, C. Lei, J. Han, and S. Pan, *$Pb_7O(OH)_3(CO_3)_3(BO_3)$: first mixed borate and carbonate nonlinear optical material exhibiting large second-harmonic generation response*, Inorg. Chem. 54 (2015), pp. 4138–4142.
[14] L. Chang, L. Wang, X. Su, S. Pan, R. Hailili, H. Yu, and Z. Yang, *A nitrate nonlinear optical crystal $Pb_{16}(OH)_{16}(NO_3)_{16}$ with a large second-harmonic generation response*, Inorg. Chem. 53 (2014), pp. 3320–3325.

[15] P. Blaha, K. Schwarz, G.K.H. Madsen, D. Kvasnicka, and J. Luitz, *WIEN2k, an augmented plane wave plus local orbitals program for calculating crystal properties*, Vienna University of Technology, Austria, 2001.
[16] D.M. Ceperley and B.I. Alder, *Ground state of the electron gas by a stochastic method*, Phys. Rev. Lett. 45 (1980), p. 566–569.
[17] J.P. Perdew, S. Burke, and M. Ernzerhof, *Generalized gradient approximation made simple*, Phys. Rev. Lett. 77 (1996), p. 3865–3868.
[18] P. Dufek, P. Blaha, and K. Schwarz, *Applications of Engel and Vosko's generalized gradient approximation in solids*, Phys. Rev. B 50 (1994), p. 7279–7283.
[19] Y. Zhao and D.G. Truhlar, *Calculation of semiconductor band gaps with the M06-L density functional*, J. Chem. Phys. 130 (2009), p. 074103.
[20] H. Xiao, J. Tahir-Kheli, and W.A. Goddard, *Accurate band gaps for semiconductors from density functional theory*, J. Phys. Chem. Lett. 2 (2011), pp. 212–217.
[21] E. Engel and S.H. Vosko, *Exact exchange-only potentials and the virial relation as microscopic criteria for generalized gradient approximations*, Phys. Rev. B 47 (1993), p. 13164–13174.
[22] F. Tran and P. Blaha, *Accurate band gaps of semiconductors and insulators with a semilocal exchange-correlation potential*, Phys. Rev. Lett. 102 (2009), p. 226401.
[23] A.H. Reshak, H. Huang, H. Kamarudin, and S. Auluck, *Alkali-metal/alkaline-earth-metal fluorine beryllium borate $NaSr_3Be_3B_3O_9F_4$ with large nonlinear optical properties in the deep-ultraviolet region*, J. Appl. Phys. 117 (2015), p. 085703.
[24] F. Wooten, *Optical properties of solid*, Academic press, New York, 1972.
[25] D.R. Penn, *Wave-number-dependent dielectric function of semiconductors*, Phys. Rev. 128 (1962), p. 2093–2097.